JOURNAL OF SYNCHROTRON RADIATION

ISSN: 1600-5775
journals.iucr.org/s

Towards a microchannel-based X-ray detector with two-dimensional spatial and time resolution and high dynamic range

Bernhard W. Adams, Anil U. Mane, Jeffrey W. Elam, Razib Obaid, Matthew Wetstein and Matthieu Chollet

J. Synchrotron Rad. (2015). **22**, 1202–1206

JOURNAL OF SYNCHROTRON RADIATION

ISSN 1600-5775

Towards a microchannel-based X-ray detector with two-dimensional spatial and time resolution and high dynamic range

Bernhard W. Adams,[a]* Anil U. Mane,[a] Jeffrey W. Elam,[a] Razib Obaid,[b] Matthew Wetstein[c] and Matthieu Chollet[d]

[a]Argonne National Laboratory, 9700 South Cass Avenue, Argonne, IL 60439, USA, [b]Physics Department, University of Connecticut, 2152 Hillside Road, U-3046 Storrs, CT 06269-3046, USA, [c]Enrico Fermi Institute, University of Chicago, 5638 South Ellis Avenue, Chicago, IL 60637, USA, and [d]Linac Coherent Light Source, 2575 Sand Hill Road, MS103, Menlo Park, CA 94025, USA. *Correspondence e-mail: adams@aps.anl.gov

Received 24 November 2014
Accepted 28 May 2015

Edited by P. A. Pianetta, SLAC National Accelerator Laboratory, USA

Keywords: high dynamic range; microchannel-based X-ray detector.

X-ray detectors that combine two-dimensional spatial resolution with a high time resolution are needed in numerous applications of synchrotron radiation. Most detectors with this combination of capabilities are based on semiconductor technology and are therefore limited in size. Furthermore, the time resolution is often realised through rapid time-gating of the acquisition, followed by a slower readout. Here, a detector technology is realised based on relatively inexpensive microchannel plates that uses GHz waveform sampling for a millimeter-scale spatial resolution and better than 100 ps time resolution. The technology is capable of continuous streaming of time- and location-tagged events at rates greater than 10^7 events per cm^2. Time-gating can be used for improved dynamic range.

1. Introduction

X-ray area detectors with a high time resolution are in increasing demand in a wide range of applications, including both imaging and scattering. Important considerations are the resolution in time and space, and the associated ranges, *i.e.* the field of view and time span covered at a given resolution. Furthermore, there is a choice between proportional and photon-counting detectors, the latter may have energy resolution, and both are subject to noise. Finally, the time resolution may be achieved through time-gating, which is often used in stroboscopic applications, or rapidly repetitive or continuous readout at some rate that determines the time resolution. These considerations, as well as the price, need to be balanced for a given application. Some examples are:

(i) CCD or CMOS sensor-array cameras. The X-rays may be converted to visible light in a scintillator, or the sensor chip may be exposed directly to the X-rays. These are relatively slow; CCDs are typically read out at rates of up to a few hundred frames per second. CMOS sensor arrays can be read out somewhat faster by restricting a region of interest, but, even so, frame rates of a few kHz are the maximum possible. Sensor areas range from about 1 to about 100 cm^2. Both CCD and CMOS cameras are mostly used in proportional (*i.e.* not photon-counting) mode.

(ii) Digital pixel-array detectors, such as the Pilatus or Eiger detectors (Dectris, http://www.dectris.com), process photon-detection events in each pixel. The data are read out in terms of digital counts of photon hits. The sensitivity of these detectors can be time-gated to about 100 ns. This is then

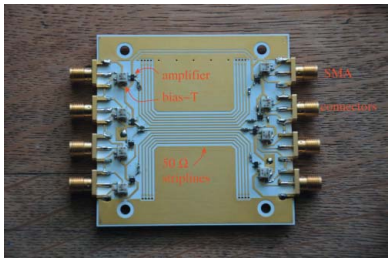

equivalent to 100 ps resolution if the synchrotron source is operating at bunch repetition periods longer than that, such as the 24-bunch mode of the Advanced Photon Source (APS) (http://www.aps.anl.gov). Some degree of energy resolution is possible by setting a detection threshold. Sensor areas up to a few 100 cm^2 are available.

(iii) Analog pixel-array detectors can handle multiple photons per gated time interval, and there are designs that can acquire multiple frames in rapid succession, which are read out summarily after the pixel buffers are full.

(iv) Detectors based on resistive charge division.

(v) A new development is the large-area picosecond photon detection (LAPPD) technology (University of Chicago, http://psec.uchicago.edu/), which detects individual photons through conversion to photoelectrons and subsequent amplification in a stack of microchannel plates (MCPs). Readout is done through an array of microwave striplines and gigahertz-waveform-sampling electronics.

The recently developed LAPPD technology has demonstrated visible-photon detection with sub-millimeter spatial resolution, and 50 to 100 ps time resolution (Adams *et al.*, 2013, 2015). It is based on a combination of a novel type of inexpensive microchannel-plate electron amplifiers (Wiza, 1979) with gigahertz-bandwidth waveform sampling. A stack of, typically, two MCPs sits atop an array of microwave striplines, and a photocathode is mounted above the stack. When a photoelectron is released from the cathode, the gain in the MCPs injects into the stripline array a short current pulse of the order of 10^6 electrons for the duration of a few hundred picoseconds. The sampled waveforms are processed digitally to extract the pulse-arrival times on both ends for the determination of photon-strike time and longitudinal position, and centroid over the striplines (which stripline was hit, with interpolation) for the transverse position.

The MCPs are produced in a novel way that has several advantages over the traditional method: the MCPs are much less expensive, more robust, live longer (in terms of extracted charge per area), and can be considerably larger (up to 20 cm × 20 cm, to date) (Mane *et al.*, 2011; Siegmund *et al.*, 2013). First, a plate cut from a boule of hollow fibers (Incom, http://www.incomusa.com), which are drawn from a type of borosilicate glass, is conformally and uniformly coated with a slightly conductive layer, and then with a layer of secondary-electron-emitter material (typically Al_2O_3 or MgO). The method used for this process is called atomic layer deposition (ALD), and is a self-terminating chemical reaction between alternatingly applied gaseous reagents. The self-terminating character of the reaction, and not diffusion into the pores, determines the layer thickness, which is therefore highly uniform throughout. Before or after the ALD coating, the two exposed planar substrates of the MCP are metalized by physical vapor deposition. In test setups, such as the one described here, an oscilloscope is used for waveform sampling. However, a real detector will use a massively parallel waveform sampler based on application-specific integrated circuits (Oberla *et al.*, 2014). A 2 × 30 channel sampler has been tested successfully (Adams *et al.*, 2013).

2. The X-ray detector

A small prototype detector based on 33 mm-diameter MCPs was built to demonstrate the adaptation of LAPPD technology to X-rays. A schematic cross-sectional view is shown in Fig. 1.

A specially prepared MCP presents the inside walls of its 20 µm pores to the incident X-rays, which, due to the 8° grazing incidence angle, are preferentially absorbed in a near-surface layer. In order to maximize the X-ray stopping power while providing a small amount of electrical conductivity for charge replenishment, this photocathode MCP has an ALD coating of tungsten oxide instead of the 'chem-II' aluminium–molybdenum oxide/aluminium oxide coating of the 'conventional' LAPPD-style MCPs (Mane & Elam, 2013). Tungsten oxide was selected for its combination of high absorption cross section for X-rays at wavelengths near 1 Å and the slight electrical conductivity of its oxide. Photoelectrons resulting from the grazing-angle X-ray absorption then have a good chance of leaving the wall material. Once inside the pore, they are extracted by a voltage of a few hundred volts, which is below the MCP gain threshold. After crossing a gap of about 5 mm, they are then further amplified in a stack of 'conventional' LAPPD-style MCPs (chem-II, 20 µm pores). All three MCPs were made from the smaller 33 mm-diameter glass substrates that are used for characterization purposes in the main LAPPD project (Adams *et al.*, 2013). Just as there, it will then be a rather straightforward matter to scale the detector size up to 20 cm × 20 cm. The advantage of direct photoelectron generation, as opposed to using a scintillator with a visible-light photocathode, is the much faster response and lack of afterglow. In future devices, the round-pore MCPs will be replaced with square-pore ones that present a flat surface to the incident X-rays.

The gain in the MCPs rises very steeply with the applied voltage. Typically, below about 700 V there is no measurable gain at all and at 1000 V the gain is of the order of 1000-fold.

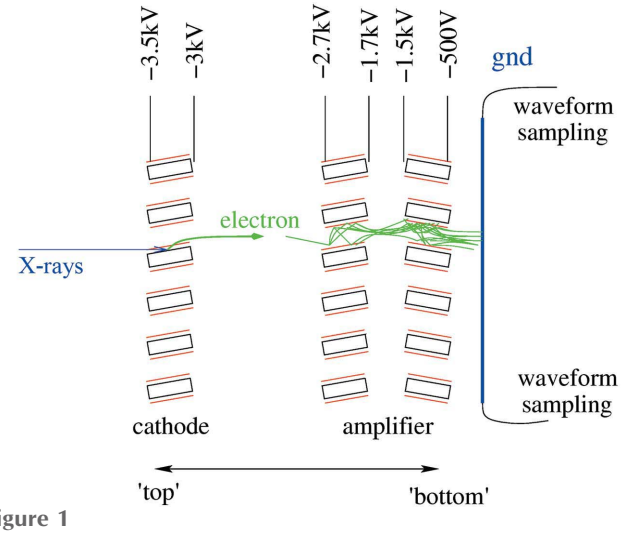

Figure 1
Schematic cross section of the X-ray detector with one MCP optimized as an X-ray photocathode and two more to amplify the photoelectron pulses.

The cathode MCP is operated below the gain threshold and does not have a layer optimized for secondary-electron emission. The applied voltage of a few 100 V serves only to extract the electrons from the pores. This lower voltage can be switched rapidly for gating the detector, and thus blanking out events that are not of interest, and that would otherwise overwhelm the gain MCPs.

Fig. 2 shows the detector assembly on an ultrahigh-vacuum flange. A glass plate for holding the MCPs in place sits atop a printed-circuit board with readout striplines, which is described below. Kapton-insulated wires bring the operating voltages to the assembly, and Teflon-insulated coaxial cables, attached *via* SMA connectors to the readout board, take the signals to SMA vacuum feedthroughs. For operation, this flange is attached to a vacuum vessel and a 20 mm diamond window on the opposite side of the vessel permits X-rays or UV light to enter and strike the cathode MCP.

The readout striplines of the prototype X-ray detectors are controlled-impedance 50 Ω lines on multilayer microwave-grade circuit-board material with the following specifications: Rogers 4350 dielectric with $\varepsilon_r = 3.48$, 196 µm (7.72 mils) thick over the internal ground plane, and a trace width of 386 µm (15.2 mils). Formulas to calculate the trace impedance and effective dielectric constant can be found in textbooks or several places on the web, such as http://microwaves101.com. With these, the effective dielectric constant ε_e of the stripline (ε_r below, vacuum above) is 2.74, and the signal propagation speed is $v_p = c(\varepsilon_e)^{-1/2} = 0.18$ mm ps^{-1}. In order to reduce the gain requirements on the MCPs, microwave amplifiers (Minicircuits type PSA4-5043+) are installed at the ends of the striplines with bias-Ts (RF/DC separators) right next to them. These amplifiers have a gain of 18.5 dB within a bandwidth of 50 MHz to 4 GHz. With them, the charge extraction from the MCPs, and therefore the recovery time after a pulse, is reduced, and high-rate operation is possible (see below). Fig. 3 shows a photograph of the anode circuit board.

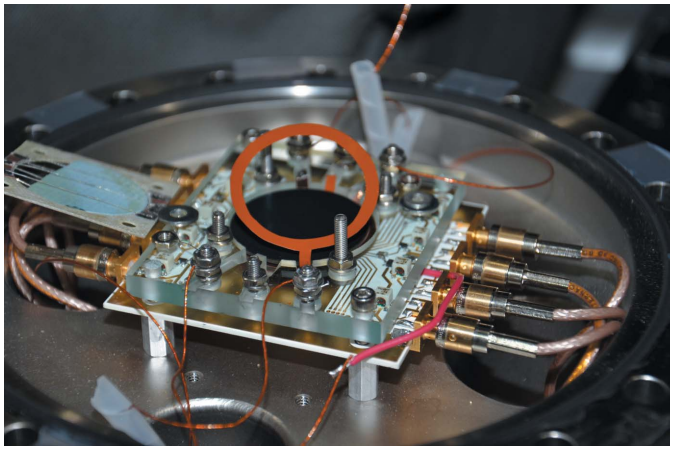

Figure 2
The detector assembly on a vacuum flange. A glass plate sits atop the anode board, and the MCPs are inserted into an aperture in it. The gain MCPs are the dark plates of 33 mm diameter, and the cathode MCP is the light-green plate with a section broken off its circular outline in a holder flipped over to the left. The high voltages are brought to the MCPs with annular-shaped pieces of metalized Kapton that have tabs sticking into grooves in the glass plate, which end in screw terminals. One such piece of metalized Kapton is shown partially lifted up.

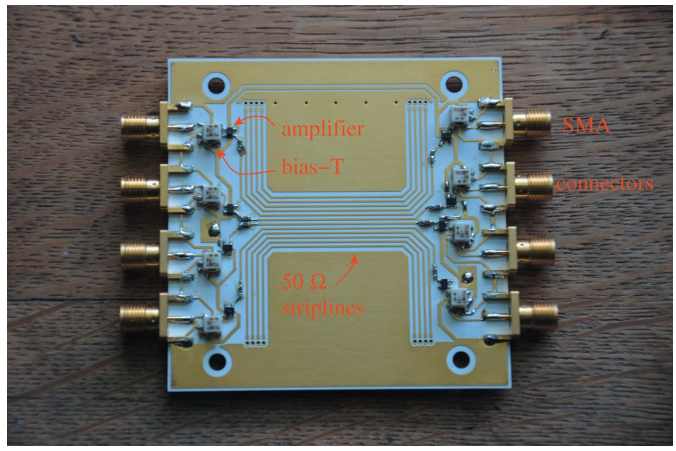

Figure 3
The anode circuit board with the amplifiers and bias-Ts for power supply.

3. Operation

Tests of the detector were performed at beamline 7-BM of the Advanced Photon Source, using X-rays of a photon energy of 10 keV. For testing purposes, the waveforms were acquired with a Tektronix DPO71604 oscilloscope (16 GHz, 50 Gs s^{-1} on four channels). Fig. 4 shows a typical pair of waveforms collected from the two ends of a stripline under X-ray irradiation.

Unlike with bare striplines, the pulses from the inverting amplifiers are positive-going. Although the rise time of the pulses is of the order of a few hundred picoseconds, their timing can be determined at a much greater accuracy using the constant-fraction technique, or template fitting, as demonstrated by Adams *et al.* (2015). Uncertainties in the timing are mainly due to (i) jitter in the gain process in the MCPs and (ii) jitter in the waveform acquisition at the ends of the striplines from sampling errors, electronic noise, *etc.* As Adams *et al.* (2015) show, the former is by far the dominant jitter and is of

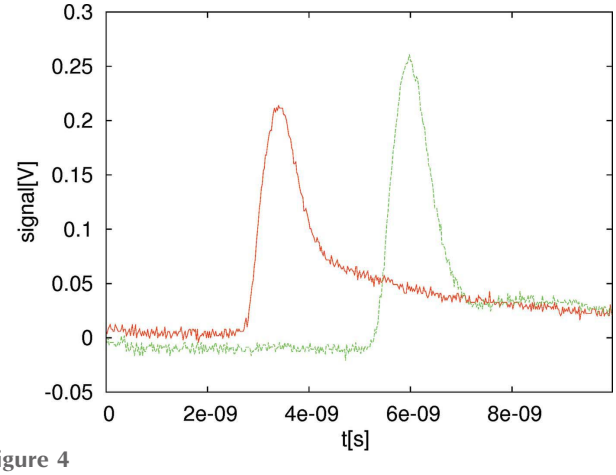

Figure 4
A typical pair of oscilloscope traces due to an X-ray photon from opposite ends of one stripline.

the order of 50–70 ps, while the latter could be brought down to about 5 ps using sophisticated waveform processing (template fitting). The determination of absolute timing, *i.e.* when a photon strikes the photocathode, is subject to both types of timing jitter, but the first, being more than ten times larger, is dominant. In contrast to this, uncertainties in the position where the photon absorption took place relative to the direction along the striplines are only due to the second type of jitter. This is due to the fact that the waveforms at both ends of a stripline originate from the same amplified pulse, regardless of when it occurs relative to the original photon strike.

Because the microwave amplifiers supply a large amount of the gain, the MCP stack can be operated at lower gain than the usual $\sim 10^6$. Consequently, a pore that has amplified a pulse will take much less time to recover than the typically observed milliseconds. This is demonstrated in Fig. 5 where the detector gives signals at the full 6.5 MHz repetition rate of the APS in its 24-bunch mode. This means that, on average, each pore produces a pulse once in 200 µs, *i.e.* at a much higher rate than usually observed with MCPs. With the four striplines of the prototype, count rates of the order of 2×10^7 s^{-1} are possible, and the rate scales linearly with the number of striplines.

For this experiment, the X-rays were slit down to a beam of 50 µm × 50 µm, thus covering about six of the pores on a 20 µm pitch. The fluctuations in peak height are due to the statistics of MCP gain. It is known, as well as demonstrated by Adams *et al.* (2013, 2015), that the pulse-height distribution from an MCP stack roughly follows an exponential distribution. Therefore, the pulse height cannot be taken as a measure of the photon energy or the number of photons simultaneously hitting the same spot. However, the gain variations are much less relevant when the detector is operated in the photon-counting regime, as is done here.

The spatial resolution is seen in the plot given in Fig. 6 where the signal arrival-time difference from the two ends of a stripline are plotted against the position x along the stripline. For this plot, 1000 waveforms like the one in Fig. 4 were acquired, and the time of each pulse was determined by the constant-fraction technique. Then, the means and r.m.s. deviations of the arrival-time differences for each x position

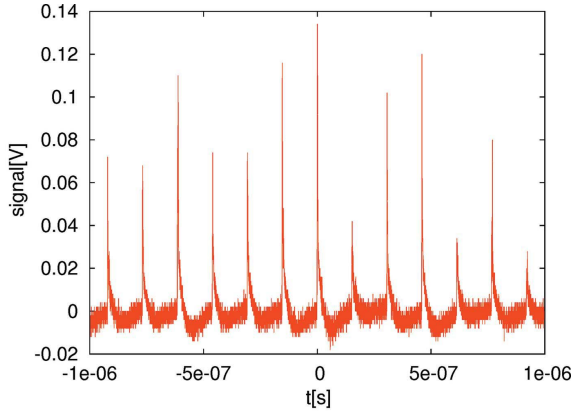

Figure 5
Signal from the detector showing the full repetition rate of the APS.

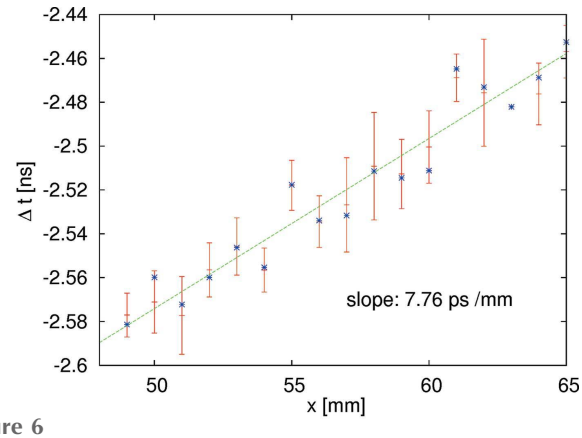

Figure 6
Plot of arrival-time difference over position x along a stripline. The slope corresponds to half the signal propagation speed.

were determined and plotted. These measurements were done for multiple lateral positions relative to the stripline. Shown are data for the X-rays hitting right above the stripline (red ticks on the centers of the error bars for the r.m.s. deviation), and for 0.5 mm off to the side (blue points). The deviations from a straight line are largely not statistical, but systematic as a comparison of the blue and red positions shows.

Because a shift in x increases the signal-travel distance in one direction, and reduces it in the other, the time difference is twice that due to the signal propagation velocity along the stripline. The measured slope of 7.76 ps mm^{-1} then corresponds to v_p = 0.26 mm ps^{-1}. The discrepancy with the expected value of 0.18 mm s^{-1} (see above) is, as yet, unexplained. The r.m.s. width of the differential timing is about 16 ps, which corresponds to a spatial resolution of 2 mm. This value could be improved substantially by application of the more sophisticated template-fitting methods described by Adams *et al.* (2015). A scan in the y direction (perpendicular to the striplines) at constant longitudinal position gives an r.m.s. width of 1 mm.

Finally, the gating capability is shown in Fig. 7, which shows the detected event rate plotted over the voltages at the top and the bottom of the cathode MCP. The top of the amplifier MCP stack was kept at −2600 V.

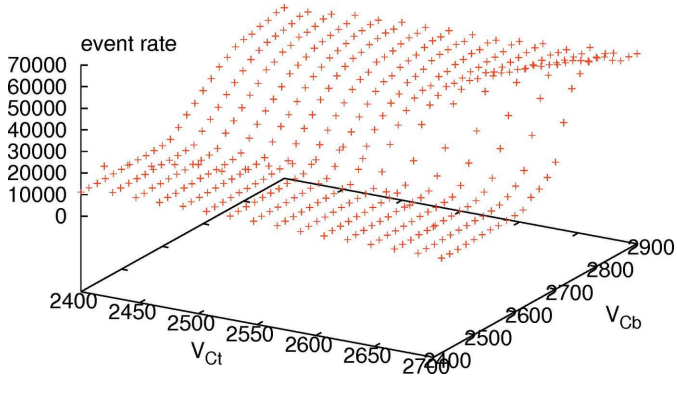

Figure 7
Detected count rate over voltages V_{Ct} and V_{Cb} at the top and bottom of the photocathode MCP. All voltages are to be multiplied by −1.

Two thresholds are visible: a very distinct threshold is the condition that the voltage V_{Cb} (Cb for 'cathode bottom') at the bottom (see Fig. 1) of the cathode MCP has to be more negative than V_{At} (At for 'amplifier top') at the top of the amplifier MCPs because, otherwise, the electrons leaving the cathode MCP are driven back to it. A less distinctive threshold is in the condition that the voltage V_{Ct} at the top of the cathode has to be more negative than V_{Cb} at the bottom, so the electrons are driven down the pores, not up. However, clearly, there is a considerable count rate even if $V_{Ct} > V_{Cb}$, which is probably due to electrons originating from parts of the pores near the bottom of the cathode MCP, and then leaving it instead of going up the pore. The plateau of about 10000 counts per second is likely due to X-rays penetrating though the cathode MCP and hitting the amplifier MCPs. This effect can be eliminated by changing the design such that the cathode MCP is not directly on top of the amplifier MCP stack but rather at some distance, and its emissions are imaged electron-optically onto the amplifier MCPs.

4. Discussion

Presented here is an X-ray detector technology that is derived from the visible-photon LAPPD technology. The latter has already demonstrated contiguous sensitive areas of 20 cm × 20 cm (Adams *et al.*, 2013). For lack of a larger photocathode MCP, the present prototype had a much smaller sensitive area of a disk with a diameter of 33 mm, but scaling to the larger size tested with visible photons should be straightforward. Such a large-area X-ray detector would be useful, for example, in time-resolved X-ray scattering applications, such as protein crystallography or powder diffraction, where X-rays coming from the sample at a wide range of angles must be monitored simultaneously The photon yield, *i.e.* the probability of detecting a signal from an X-ray photon, was not tested. This probability is given by the X-ray absorption probability in the cathode MCP, and the probability of subsequent photoelectron escape. The current cathode MCP has round pores, just like the gain MCPs. Test samples of glass plates with rectangular pores have recently been produced. Once functionalized as MCPs, these will offer a flat surface for a much better defined incidence angle than those with round pores. It is expected that this will greatly improve the photon yield.

The spatial resolution is not as good as that of typical pixel-array detectors, but can be improved by going to striplines printed on a dielectric with a higher value of ε_r, for example, GaAs with $\varepsilon_r \approx 13$. This will both permit a finer pitch of the striplines and will slow down the pulses along the striplines, so a higher spatial resolution is obtained from a given time resolution with about 16 ps r.m.s. spread. Compared with pixel-array detectors, much larger areas can be covered. Furthermore, it is not necessary to gate the detector. Rather, a continuous stream of time- and location-tagged events can be acquired. With the built-in amplifiers, the MCP gain can be lowered to achieve rapid recovery. The detector can then sustain high data rates of at least 6.5×10^6 events per second and per stripline. Applications of this capability are in cases where a high time resolution of nonrepetitive events is required. These are not amenable to stroboscopic measurements that could be performed with time-gating. Examples are imaging of turbulent flow or time-correlation spectroscopy (speckle interferometry) at widely varying time scales and a high dynamic range of intensities.

Acknowledgements

This work was supported by the US Department of Energy, Office of Basic Energy Sciences under Contract No. DE-AC02-06CH11357, and under LDRD 2011-067-N0. We would also like to thank Dr Alan Kastengren for his support at the beamline. This work would not have been possible without the foundation laid by the LAPPD team (University of Chicago). Finally, we would like to thank Professor Henry Frisch for valuable comments and support of this project as a spin-off from the LAPPD collaboration.

References

Adams, B., Chollet, M., Elagin, A., Oberla, E., Vostrikov, A., Wetstein, M., Obaid, R. & Webster, P. (2013). *Rev. Sci. Instrum.* **84**, 061301.

Adams, B., Elagin, A., Frisch, H., Obaid, R., Oberla, E., Vostrikov, A., Wagner, R., Wang, J. & Wetstein, M. (2015). *Nucl. Instrum. Methods Phys. Res. A.* **795**, 1–11.

Mane, A. U. & Elam, J. W. (2013). *Proc. SPIE*, **8818**, 88180M.

Mane, A. U., Peng, Q., Wetstein, M. J., Wagner, R. G., Frisch, H. J., Siegmund, O. H. W., Minot, M. J., Adams, B. W., Chollet, M. C. & Elam, J. W. (2011). *Proc. SPIE*, **8031**, 80312H.

Oberla, E., Genat, J.-F., Grabas, H., Frisch, H., Nishimura, K. & Varner, G. (2014). *Nucl. Instrum. Methods Phys. Res. A*, **735**, 452–461.

Siegmund, O., Richner, N., Gunjala, G., McPhate, J., Tremsin, A. S., Frisch, H. J., Elam, J., Mane, A., Wagner, R., Craven, C. A. & Minot, M. J. (2013). *Proc. SPIE*, **8859**, 88590Y.

Wiza, J. L. (1979). *Nucl. Instrum. Methods*, **162**, 587–601.